Lattice determination of the topological susceptibility slope χ' of $2d$ CP^{N-1} models at large N

Claudio Bonanno[*]

INFN Sezione di Firenze, Via Giovanni Sansone 1, I-50019 Sesto Fiorentino, Firenze, Italy

We compute the topological susceptibility slope χ', related to the second moment of the two-point correlator of the topological charge density, of $2d$ CP^{N-1} models for $N = 5$, 11, 21 and 31 from lattice Monte Carlo simulations. Our strategy consists in performing a double limit: first, we take the continuum limit of χ' at fixed smoothing radius in physical units; then, we take the zero-smoothing-radius limit. Since the same strategy can also be applied to $4d$ gauge theories and full QCD, where χ' plays an intriguing theoretical and phenomenological role, this work constitutes a step toward the lattice investigation of this quantity in such models.

I. INTRODUCTION

The space of gauge field configurations with finite Euclidean action can be divided in disconnected sectors characterized by an integer number, the topological charge

$$Q = \int d^d x\, q(x) \in \mathbb{Z}, \tag{1}$$

where d is the space-time dimension and $q(x)$ is the topological charge density, which is a local function of the gauge fields. Many intriguing nonperturbative properties of $4d$ non-Abelian gauge theories, as well as many phenomenological aspects of the Standard Model (and beyond), are related to the topology of gauge fields.

A particularly interesting topological quantity to consider is the two-point correlation function of $q(x)$ [1–9]:

$$\tilde{G}(p^2) \equiv \int d^d x\, e^{ip\cdot x} G(x), \tag{2}$$

where $G(x)$ is the Euclidean space-time correlator

$$G(x - y) \equiv \langle q(x)q(y) \rangle = \langle q(x - y)q(0) \rangle. \tag{3}$$

In Fourier space, the two-point correlator is a function of $p^2 \equiv p_\mu p_\mu$, being $q(x)$ a CP-odd operator, and it is

*claudio.bonanno@fi.infn.it

customary to Taylor expand it around $p^2 = 0$ in powers of p^2:

$$\tilde{G}(p^2) = \sum_{n=0}^{\infty} (-1)^n G_{2n} p^{2n}, \tag{4}$$

where the expansion coefficients G_{2n} are proportional to the even moments of the correlator $G(x)$:

$$G_{2n} \equiv \frac{1}{d^n (2n)!} \int d^d x\, |x|^{2n} G(x). \tag{5}$$

The leading-order coefficient of the expansion in Eq. (4) is nothing but the integral of $G(x)$, which is equal to the well-known *topological susceptibility*

$$\chi \equiv \lim_{V \to \infty} \frac{\langle Q^2 \rangle}{V}, \tag{6}$$

as it can be easily derived from the translation invariance of the correlator:

$$\begin{aligned}
\tilde{G}(0) = G_0 &= \int d^d x \langle q(x)q(0) \rangle \\
&= \lim_{V \to \infty} \frac{1}{V} \int d^d x\, d^d y \langle q(x)q(y) \rangle \\
&= \lim_{V \to \infty} \frac{\langle Q^2 \rangle}{V} = \chi.
\end{aligned}$$

The object of investigation of the present paper is, instead, the next-to-leading-order term in the momentum expansion of $\tilde{G}(p^2)$, the so-called *topological susceptibility slope χ'*:

$$\chi' \equiv -\frac{d\tilde{G}(p^2)}{dp^2}\bigg|_{p^2=0}$$
$$= \int d^d x \frac{|x|^2}{2d} \langle q(x)q(0)\rangle. \qquad (7)$$

This quantity is extremely interesting from a theoretical and from a phenomenological point of view. In SU(N) pure-gauge theories, the susceptibility slope controls the internal consistency of the Witten-Veneziano mechanism [10–12]. More precisely, for the Witten-Veneziano equation for the η' mass to be valid, $|\chi'| \ll \chi/m_{\eta'}^2$ must hold in the large-N limit. In QCD, instead, the value of the susceptibility slope in the chiral limit (which is expected to be nonvanishing, unlike the chiral limit of χ) is related to the "spin content" of the proton via the so-called U(1) Goldberger-Treiman relation [13–17].

However, in spite of its interesting theoretical and phenomenological role, the computation of χ' has been quite disregarded for what concerns the lattice approach, especially if compared with the topological susceptibility, which has been widely investigated by numerical Monte Carlo (MC) simulations both in pure-gauge theories 38–4,18]] and in full QCD [32,39–48], but also in lower-dimensional toy models [49–60].

As a matter of fact, while a prediction for χ' is available in QCD from chiral perturbation theory [61] and from the QCD sum rule [16,62–64] [which also provides an estimation of χ' in the pure SU(3) gauge theory [16,63]], only preliminary attempts to compute it from the lattice can be retrieved in the literature; cf. Refs. [65–68].

The goal of the present work is thus to fill a gap in the lattice literature by making progress in the numerical computation of χ'. To this end, we start our investigation from the simpler framework offered by large-N 2d CP^{N-1} models [4,69–71], which are interesting quantum field theories that have been extensively used as a theoretical laboratory for QCD. On one hand, they are much cheaper to simulate on the lattice with Monte Carlo methods. On the other hand, they offer the possibility to obtain analytical results about topological quantities in the large-N limit through the $1/N$ expansion, which can be compared to lattice determinations.

Since the methods that will be applied to these models to compute χ' are rather general and can be applied also to SU(N) pure Yang-Mills or to full QCD, the main purpose of this work is to show the feasibility and the solidity of our numerical strategies to obtain χ' from lattice simulations. Therefore, this paper constitutes a step toward a deeper investigation of χ' from the lattice also in 4d gauge theories.

This paper is organized as follows. In Sec. II we briefly recall the continuum definition of CP^{N-1} models and the available analytic predictions for the $1/N$ expansion of χ'. In Sec. III we outline our lattice setup and MC algorithms, as well as our numerical strategies to compute χ'. In Sec. IV

we show our results for χ' for $N = 5, 11, 21$ and 31 and we compare them with large-N analytic predictions. Finally, in Sec. V we draw our conclusions and discuss future outlooks of this work.

II. CONTINUUM 2d CP^{N-1} MODELS AND THE ANALYTIC $1/N$ EXPANSION OF χ'

The continuum Euclidean action of 2d CP^{N-1} models can be written as [69,70]

$$S[z, A] = \int d^2x \left[\frac{N}{g} \bar{D}_\mu \bar{z}(x) D_\mu z(x) \right], \qquad (8)$$

where the complex scalar field $z = (z_1, \ldots, z_N)$ is an N-component vector with unit norm $\bar{z}z = 1$ and where $D_\mu \equiv \partial_\mu + iA_\mu$ is the ordinary U(1) covariant derivative. The field $A_\mu(x)$ is a nonpropagating U(1) gauge field which can be integrated out and expressed in terms of z [4,70], but this formulation is more convenient for the purpose of the lattice discretization. Finally, the coupling constant g is the 't Hooft coupling, and it is kept constant as N is varied.

The integer-valued topological charge, instead, reads [69,70]

$$Q = \int d^2x q(x) = \frac{1}{2\pi} \epsilon_{\mu\nu} \int d^2x \partial_\mu A_\nu(x) \in \mathbb{Z}, \quad (9)$$

where $q(x)$ is the topological charge density, which is used to define χ' as in Eq. (7).

In the large-N limit, it is possible to perform an analytic computation of the susceptibility slope within the framework of the $1/N$ expansion. In Ref. [72], the leading-order (LO) and the next-to-leading-order (NLO) terms in the $1/N$ expansion were computed:

$$\chi' = -\frac{3}{10\pi}\frac{1}{N} + e'_2 \frac{1}{N^2} + O\left(\frac{1}{N^3}\right), \qquad (10)$$

where the NLO coefficient is $e'_2 \simeq 1.53671$.

III. NUMERICAL SETUP

In this section we discuss our numerical setup by outlining the adopted discretizations for the main quantities of interest, the adopted MC algorithms and the strategies we followed to compute the topological susceptibility slope χ'.

A. Lattice discretization

We discretize (8) on a square periodic lattice (we will discuss other boundary conditions later) with L^2 sites and lattice spacing a by means of the $O(a)$ tree-level Symanzik-improved lattice action [50]:

$$S_L = -2N\beta_L \sum_{x,\mu} \{c_1 \text{Re}[\bar{U}_\mu(x)\bar{z}(x+\hat{\mu})z(x)]$$

$$+c_2 \text{Re}[\bar{U}_\mu(x+\hat{\mu})\bar{U}_\mu(x)\bar{z}(x+2\hat{\mu})z(x)]\}, \quad (11)$$

where β_L is the lattice bare coupling and where we introduced site variables $z(x)$ satisfying $\bar{z}(x)z(x) = 1$ and U(1) link variables $U_\mu(x)$ satisfying $\bar{U}_\mu(x)U_\mu(x) = 1$ as well (no sum on μ is implied). The choice of the improved lattice action allows one to exactly cancel out logarithmic corrections to the leading-order $O(a^2)$ behavior of the finite-lattice-spacing corrections to the continuum limit, improving convergence.

Lattice configurations are updated by means of the standard overrelaxation (OR) and over-heat-bath (HB) [50] local algorithms. In particular, our standard updating step is made of four lattice sweeps of OR, followed by one sweep of HB. In the following, we will refer to this combination as the "standard algorithm."

The continuum topological charge (9) can be discretized by several different definitions. In this work we will consider the *geometric* definition built in terms of the gauge links [50]:

$$Q_L = \sum_x q_L(x) = \frac{1}{2\pi} \sum_x \text{Im}\{\log[\Pi_{01}(x)]\}, \quad (12)$$

with $\Pi_{\mu\nu}(x) \equiv U_\mu(x)U_\nu(x+a\hat{\mu})\bar{U}_\nu(x+a\hat{\mu})\bar{U}_\nu(x)$ the plaquette and $q_L(x)$ the lattice topological charge density. This definition has the property of always resulting in an integer number: $Q_L \in \mathbb{Z}$. However, it being affected by *dislocations* [51,73], UV fluctuations at the scale of the lattice spacing that can make identifying the correct winding number ambiguous, it is customary to compute the lattice topological charge after smoothing, using one's favorite algorithm, in order to dump short-distance fluctuations. We postpone a more detailed discussion on smoothing methods to Sec. III C, where we will cover this topic more thoroughly in relation with χ'.

In order to fix the physical scale, we introduce the *second-moment correlation length*

$$\xi^2 \equiv \frac{1}{\int G_P(x)d^2x} \int G_P(x)\frac{|x|^2}{4}d^2x, \quad (13)$$

where $G_P(x)$ stands for the two-point connected correlator of $P_{ij}(x) \equiv z_i(x)\bar{z}_j(x)$:

$$G_P(x) \equiv \langle P_{ij}(x)P_{ij}(0)\rangle - \frac{1}{N}. \quad (14)$$

Introducing the dimensionless quantity $\xi_L = \xi/a$, it is possible to compute it from the lattice as [74]

$$\xi_L^2 = \frac{1}{4\sin^2(\pi/L)}\left[\frac{\tilde{G}_P^{(L)}(0,0)}{\tilde{G}_P^{(L)}(2\pi/L,0)} - 1\right], \quad (15)$$

where $\tilde{G}_P^{(L)}(p_\mu)$ is the Fourier transform of $G_P^{(L)}(x)$, the straightforward lattice definition of $G_P(x)$.

In the continuum limit $a \to 0$, approached by taking $\beta_L \to \infty$, the correlation length expressed in lattice units diverges as a. Thus, it is possible to trade the vanishing lattice spacing limit for the $\xi_L \to \infty$ one. Therefore, finite-lattice-spacing corrections to the continuum expectation value of a certain observable $\langle\mathcal{O}\rangle_{\text{cont}}$ can be expressed as

$$\langle\mathcal{O}\rangle_{\text{lat}}(\xi_L) = \langle\mathcal{O}\rangle_{\text{cont}} + \frac{c}{\xi_L^2} + o\left(\frac{1}{\xi_L^2}\right). \quad (16)$$

B. Topological freezing and parallel tempering on boundary conditions

At large N and close to the continuum limit, it is well known that standard updating algorithms suffer for a severe *topological critical slowing down* [23,24,30,35,37,44,53,57]. This means that the autocorrelation time of the topological charge, i.e., the number of updating steps needed to generate two field configurations with uncorrelated values of Q, rapidly grows when ξ_L and/or N is large. Numerical evidence suggests that this growth is exponential in N and ξ_L [23,30,53,57]. This in practice results in the so-called *topological freezing*; i.e., the Monte Carlo history of the topological charge gets stuck in a fixed topological sector and eventually no topological fluctuation is observed, requiring unfeasible long simulations to achieve a proper sampling of the path integral.

To deal with this computational problem we adopted the *parallel tempering on boundary conditions* (PTBC) algorithm to mitigate the effects of topological freezing. Originally proposed by Hasenbusch [55] for $2d$ CP^{N-1} models (see also [58]) and recently implemented also for $4d$ pure-gauge Yang–Mills theories [35,37], this algorithm has proven to be extremely effective in mitigating the effects of topological freezing at large N by reducing the autocorrelation time of Q by up to several orders of magnitude. Here, we use the same algorithmic setup of Ref. [58].

We consider N_r copies of the discretized theory outlined in Sec. III A. Each replica differs from the others only for the boundary conditions imposed on a small subregion of the lattice D, called *the defect*. Away from the defect, boundary conditions are periodic as usual. In practice, we rewrite the lattice action (11) as

$$S_L^{(r)} = -2N\beta_L \sum_{x,\mu}\{k_\mu^{(r)}(x)c_1\text{Re}[\bar{U}_\mu(x)\bar{z}(x+\hat{\mu})z(x)]$$

$$+ k_\mu^{(r)}(x+\hat{\mu})k_\mu^{(r)}(x)c_2$$

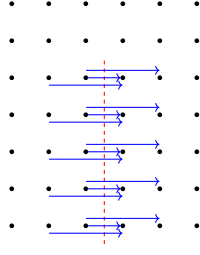$$\times \text{Re}[\bar{U}_\mu(x+\hat{\mu})\bar{U}_\mu(x)\bar{z}(x+2\hat{\mu})z(x)]\},$$

FIG. 1. Figure taken from Ref. [58]. The dashed line represents the defect D; solid arrows represent links or product of links appearing in the Symanzik action (11) which orthogonally cross the defect line and get suppressed as factors of $c(r)$.

where the coefficients

$$k_\mu^{(r)}(x) \equiv \begin{cases} c(r), & x \in D \wedge \mu = 0; \\ 1, & \text{otherwise} \end{cases} \qquad (17)$$

are used to effectively implement the chosen boundary conditions on the defect. In particular, the coefficients $c(r)$ are chosen so as to interpolate among periodic boundaries $c(0) = 1$ and open boundaries $c(N_r - 1) = 0$. In our setup, we chose a simple linear interpolation: $c(r) = 1 - r/(N_r - 1)$. The defect D is set on the $\mu = 1$ boundary and is L_d sites long. A pictorial representation of the defect and of the sites or links affected by its presence is depicted in Fig. 1.

Each replica is evolved independently using the standard algorithm earlier outlined. After the updates, field configurations are swapped among adjacent copies $(r, r + 1)$, so that the field configuration can diffuse from the periodic replica to the open one and vice versa, in a random-walk fashion. This way, the fast decorrelation of the topological charge achieved in the replica with open boundaries is transferred to the periodic copy, resulting in a strong reduction of the autocorrelation time of Q. The advantage of parallel tempering is that any physical observable can be computed on the periodic replica, thus avoiding technical complications related to finite size effects when computing correlators in open lattices.

The efficiency of the algorithm can be further improved by translating the periodic replica after the updates and the swaps and by alternating updating sweeps over the full lattice with updating sweeps over small sublattices centered around the defect. These two ingredients allow one, respectively, to move the position where new topological excitations are created or annihilated and to increase the number of topological fluctuations that are created or annihilated (since they are mostly located in the neighborhood of the defect).

The number of replicas N_r and the size of the defect L_d are calibrated through short test runs in order to ensure that no swap acceptance $p(r, r + 1)$ is smaller than $\sim 30\%$. In all cases, this was sufficient to ensure that a single field configuration uniformly explores all boundary conditions

and does a random walk among the two extremes of the replica chain.

C. Computation of χ' from the lattice

As mentioned in the previous section, to properly define the physical topological background of a lattice configuration, smoothing methods such as cooling [73,75–80], stout smearing [81,82] or gradient flow [83,84] need to be employed to damp UV fluctuations. All choices give consistent results when properly matched to each other [80,85,86].

Such algorithms iteratively bring a configuration closer to a local minimum of the lattice action and smooth gauge fields up to a certain distance known as the *smoothing radius* r_s, which is proportional to the square root of the amount of smoothing performed [83,84]. Since this procedure only dumps UV fluctuations at length scales $\lesssim r_s$, smoothing methods are expected to leave the global topological content of the field configuration unaltered.

As a matter of fact, lattice gluonic definitions of the topological charge like (12) reach a plateau after a certain amount of smoothing. Therefore, the choice of the number of smoothing steps is not critical when one is interested in, e.g., the global topological charge Q or the topological susceptibility $\chi \propto \langle Q^2 \rangle$.

The situation is different when dealing with objects like the topological charge density correlator (3). Indeed, if on one hand smoothing is necessary to correctly identify the true topological background of a configuration, on the other hand smoothing unavoidably modifies the short-distance behavior of $G(x)$, which is only properly recovered in the zero-smoothing limit. Therefore, to reliably compute topological quantities such as χ', it is of the utmost importance to ensure that no relevant physical contribution coming from short-distance fluctuations is lost due to the smoothing procedure.

For this reason, to extract the physical value of χ' from lattice field configurations, we follow the same strategy applied also in Ref. [8] to compute the topological charge density correlator: first, we perform the continuum limit fixing the smoothing radius r_s in physical units; then, we extrapolate our results for finite r_s toward the zero-smoothing limit $r_s \to 0$.

In a $2d$ theory, χ' is a dimensionless quantity that can be discretized on a periodic lattice as

$$\chi'_L \equiv \frac{1}{4} \left\langle \sum_x d^2(x, 0) q_L(x) q_L(0) \right\rangle, \qquad (18)$$

where $q_L(x)$ is the lattice topological charge density in Eq. (12) and $d(x, y)$ is the shortest distance between lattice sites $x = (x_0, x_1)$ and $y = (y_0, y_1)$:

TABLE I.　Summary of simulation parameters. The PTBC algorithm was employed for $N = 21, 31$, while $N = 5, 11$ were simulated with the standard algorithm. Measures were taken every ten updating steps for the standard algorithm, and at each step for parallel tempering runs. Total collected statistics is expressed in millions (M).

N	β_L	L	ξ_L	L/ξ_L	N_r	L_d	Max no. cooling steps	Statistics (M)
5	1.00	200	13.419(37)	14.9			110	17.5
	1.05	300	18.08(12)	16.6			200	6.9
	1.10	400	24.65(21)	16.2			370	4.7
11	0.75	105	5.499(27)	19.1			120	3.5
	0.77	140	6.369(67)	22.0			155	7.5
	0.79	140	6.987(67)	20.0			195	7.5
	0.848	220	9.90(12)	22.2			405	6.7
21	0.66	88	4.2129(78)	20.9	9	5	250	10.7
	0.68	102	4.7561(99)	21.4	10	6	320	10.7
	0.70	114	5.422(15)	21.0	11	6	415	5.9
	0.718	128	6.030(13)	21.2	11	6	515	9.5
	0.741	150	6.979(11)	21.4	11	6	690	22.4
31	0.58	72	2.8518(38)	25.2	10	4	110	24.0
	0.60	82	3.2409(75)	25.3	10	4	140	8.7
	0.62	92	3.6731(52)	25.0	10	4	180	7.2
	0.715	172	6.585(37)	26.1	13	7	585	2.3

$$d^2(x, y) = \sum_{\mu=0,1} d_\mu^2(x, y),$$

$$d_\mu^2(x, y) = \begin{cases} (x_\mu - y_\mu)^2, & |x_\mu - y_\mu| < L/2, \\ [L - (x_\mu - y_\mu)]^2, & |x_\mu - y_\mu| > L/2. \end{cases} \quad (19)$$

We compute χ'_L on the periodic replica after smoothing the field configuration. To this end, we adopt cooling for its numerical cheapness. A single cooling step is achieved aligning, site per site and link by link, each variable $z(x)$ and $U_\mu(x)$ to their relative local force. Since the action that is used to compute local forces during cooling needs not to be the same used for the Monte Carlo sampling [86], we adopt the nonimproved action to this end [i.e., action (11) with $c_1 = 1$ and $c_2 = 0$].

To extrapolate finite-ξ_L results of χ'_L toward the continuum limit at fixed smoothing radius, it is sufficient to consider determinations obtained for the same value of

$$\frac{n_{\text{cool}}}{\xi_L^2} \propto \left(\frac{r_s}{\xi}\right)^2, \quad (20)$$

since the smoothing radius $r_s \propto a\sqrt{n_{\text{cool}}}$:

$$\chi'_L\left(\xi_L, \frac{n_{\text{cool}}}{\xi_L^2}\right) = \chi'\left(\frac{n_{\text{cool}}}{\xi_L^2}\right) + c\xi_L^{-2} + o(\xi_L^{-2}), \quad (21)$$

where the coefficient c, in principle, may depend on the value of n_{cool}/ξ_L^2.

Finally, we extrapolate the continuum extrapolations $\chi'(n_{\text{cool}}/\xi_L^2)$ appearing in the rhs of Eq. (21) toward the *zero-cooling* limit according to the law

$$\chi'\left(\frac{n_{\text{cool}}}{\xi_L^2}\right) = \chi' + k\frac{n_{\text{cool}}}{\xi_L^2} + o\left(\frac{n_{\text{cool}}}{\xi_L^2}\right), \quad (22)$$

where χ' in the rhs of Eq. (22) represents our final result for the susceptibility slope.

To justify Eq. (22), we can rely on the argument given in Ref. [8] for the Wilson flow. Within the gradient flow framework, it is possible to express expectation values of flowed operators in terms of expectation values of unflowed operators via the operator product expansion (OPE). In the OPE series, the contribution of higher-dimensional operators is compensated by suitable powers of the flow time τ_{flow}. In particular, when considering $q(x)q(0)$, the first correction to the zero-flow result is expected to be linear in τ_{flow} [8]. Since the numerical equivalence between gradient flow and cooling and the existence of the linear proportionality $n_{\text{cool}} \propto \tau_{\text{flow}}$[1] [85] have been established, we expect to observe a linear dependence of $\chi'(n_{\text{cool}}/\xi_L^2)$ on n_{cool}/ξ_L^2 [see also Ref. [60] for a similar discussion concerning the linear zero-cooling extrapolation of $\chi(n_{\text{cool}})$ for the $2d$ CP[1] model].

IV. RESULTS

In Table I we summarize all performed simulations, along with the total collected statistics and the maximum number of cooling steps computed for each simulation point.

---

[1]For example, in the $4d$ SU(3) pure-gauge theory, the correspondence $n_{\text{cool}} = 3\tau_{\text{flow}}$ holds adopting the Wilson gauge action [85].
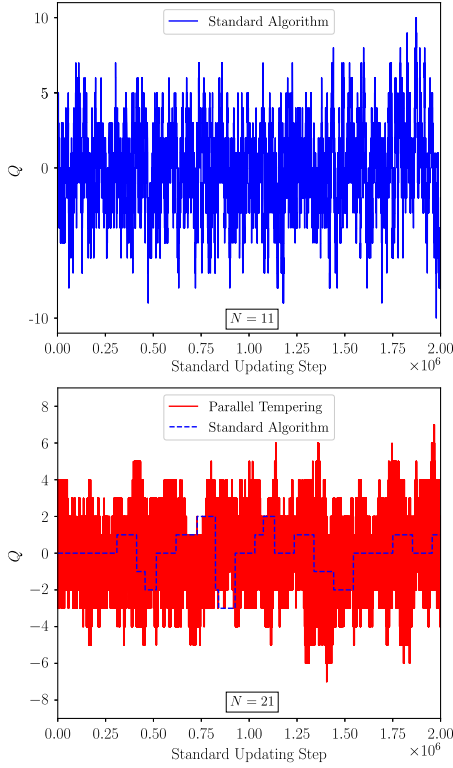
FIG. 2. Monte Carlo history of the topological charge Q. Plot refers to $N = 11$, $\beta_L = 0.848$ (top) and $N = 21$, $\beta_L = 0.741$ (bottom). Monte Carlo time for the PTBC algorithm has been expressed in units of standard updates by scaling for the number of replicas. Shown time windows correspond to, respectively, ~14% and ~10% of the total collected statistics.

Simulations for $N = 21$ and 31 where carried on adopting the PTBC algorithm, while for $N = 5$ and 11 standard updating algorithms were sufficient to easily decorrelate the topological charge. Illustrative examples are shown in Fig. 2. In the top plot we show the Monte Carlo history of the topological charge Q for $N = 11$ and $\beta_L = 0.848$. The integer charge Q is obtained computing the geometric definition Q_L in Eq. (12) after 30 cooling steps. In this case, the standard algorithm allows a uniform exploration of different topological sectors. In the bottom plot we show a comparison between the Monte Carlo evolutions of Q obtained with the PTBC algorithm and the standard one for $\beta_L = 0.741$ at $N = 21$. As it can be appreciated, while the standard algorithm suffers for much longer autocorrelation times, the PTBC algorithm allows much more fluctuations of the topological charge during the same Monte Carlo time.

This aspect is crucial to correctly compute χ'_L. As a matter of fact, although the topological charge density fluctuates even in the $Q = 0$ sector, the values obtained for χ'_L restricting to subensembles with fixed topological
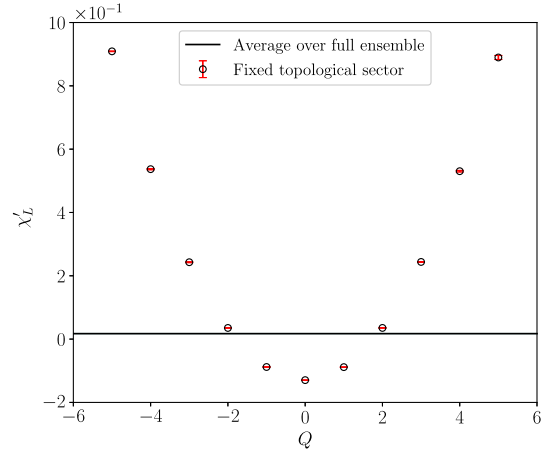

FIG. 3. Results for χ'_L computed on subensembles with fixed topological charge Q as a function of the topological background. Horizontal line displays the result obtained averaging over the full ensemble. Error bars are not visible at this scale. Plot refers to $N = 21$, $\beta_L = 0.741$, and $n_{\text{cool}} = 200$.

charge are quite different from the one obtained by taking the mean over the full ensemble, as can be observed from Fig. 3.

For what concerns the magnitude of finite-size effects, in the large-N limit two constraints have to be satisfied in order to have them under control: $L/\xi_L \gg 1$ and $(L/\xi_L)^2/N \gg 1$, as discussed in Ref. [87] (see also [58] for a related discussion about this condition). In practice, it is sufficient to ensure $(L/\xi_L)^2/N \gtrsim 20$ to have no significant systematic error related to finite volume [57,58]. Satisfying this condition required $L/\xi_L \gtrsim 15$–25 for the values of N we explored. We show an illustrative example of the magnitude of finite size effects on χ'_L for $N = 11$ in Fig. 4.
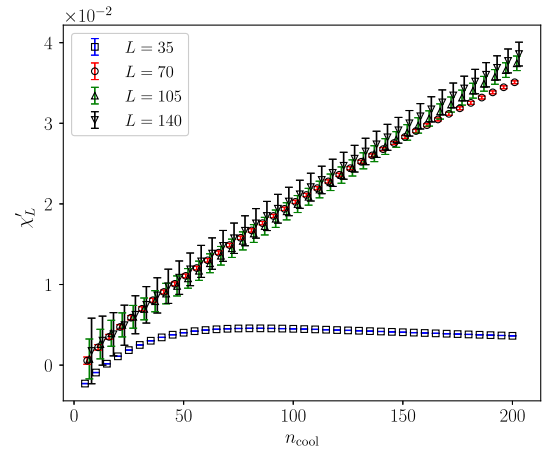

FIG. 4. Dependence of χ'_L on the lattice size L for several values of n_{cool}. Plot refers to $N = 11$ and $\beta_L = 0.77$. Points referring to the same value of n_{cool} have been slightly shifted.
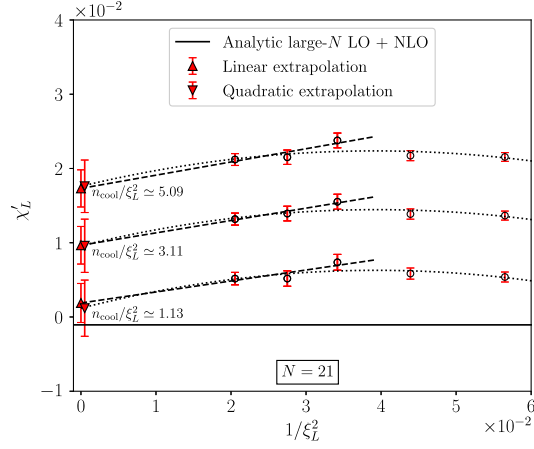
FIG. 5. Examples of extrapolation toward the continuum limit $\xi_L \to \infty$ of χ_L at fixed smoothing radius for $N = 21$ and for three values of $n_{\rm cool}/\xi_L^2$.

FIG. 7. Extrapolation toward the zero-cooling limit $n_{\rm cool}/\xi_L^2 \to 0$ of $\chi'(n_{\rm cool}/\xi_L^2)$ for $N = 21$ with a linear function in $n_{\rm cool}/\xi_L^2$. The full point represents our final result.

A. Double extrapolation—Example for $N = 21$

In this section we exemplify, for $N = 21$, the procedure followed to achieve the double extrapolation of χ' toward the continuum and the zero-cooling limit.

The first step is to extrapolate our data for χ_L' computed at fixed value of $n_{\rm cool}/\xi_L^2$ toward the continuum limit according to Eq. (21). We performed a linear fit in $1/\xi_L^2$ considering the three largest correlation lengths available, but we also checked that performing the best fit in the whole available range gave exactly the same results within errors if further $O(1/\xi_L^4)$ corrections are taken into account; cf. Fig. 5. We thus conclude that a linear fit in $1/\xi_L^2$ to the three finest lattice spacings gives a solid continuum extrapolation. As a side note, we observe that no significant dependence on $n_{\rm cool}/\xi_L^2$ of the magnitude of corrections to the continuum limit is observed.
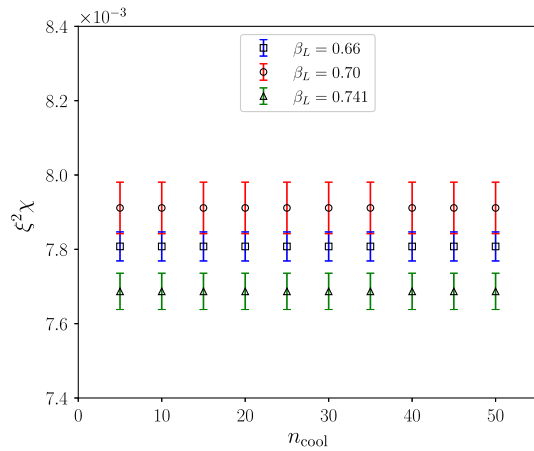

FIG. 6. Behavior of the topological susceptibility $\xi^2\chi$ as a function of $n_{\rm cool}$ for three values of β_L explored at $N = 21$ (the largest, the smallest and the middle one).

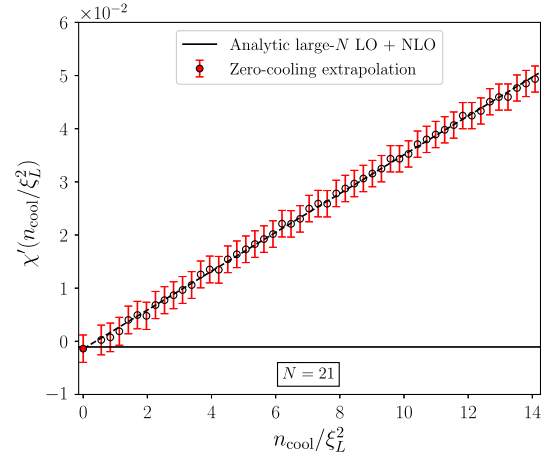Once the continuum limit is taken, we can extrapolate our continuum results toward the zero-cooling limit by performing a linear best fit in $n_{\rm cool}/\xi_L^2$, according to Eq. (22). As can be seen from Fig. 7, our χ' continuum extrapolations at finite smoothing radius are perfectly described by a linear law in $n_{\rm cool}/\xi_L^2 \propto (r_s/\xi)^2$, in agreement with our expectations. For the purpose of comparison, in Fig. 6 we also report the LO + NLO large-N analytic prediction of Eq. (10).

Concerning the choice of the fit range in this case, the lower bound was fixed to $n_{\rm cool}/\xi_L^2 \sim 0.56$, corresponding to $n_{\rm cool} = 10$ for the smallest explored correlation length. As a matter of fact, we observed that $n_{\rm cool} \geq 10$ is enough to observe a plateau in the determinations of the topological susceptibility at finite ξ_L as a function of $n_{\rm cool}$ for all simulated points; cf. Fig. 6. Therefore, this choice ensures that we are correctly identifying the topological background of the configurations for all the values of $n_{\rm cool}$ and ξ_L employed in our analysis.

As for the upper bound of the fit range, we observe that our results are in perfect agreement with a linear behavior in a wide range of values of $n_{\rm cool}/\xi_L^2$, up to $n_{\rm cool}/\xi_L^2 \sim 14$; see Fig. 7. This is nontrivial, as this value corresponds to $n_{\rm cool} = 250$ and $n_{\rm cool} = 690$ for, respectively, the smallest and largest ξ_L investigated at this value of N. Reducing the fit range by choosing a smaller upper bound resulted in no relevant change in the obtained extrapolation. In any case, we incorporated any small variation observed into our final error, displayed as a full point and a shaded area in Fig. 8.

As a final remark, we recall that, in order to correctly keep into account correlations among continuum extrapolations obtained for different values of $n_{\rm cool}/\xi_L^2$, we repeated the analysis described in this section for 5000 different bootstrap resamples for each ξ_L, each one having the same size of the original sample. Thus, our results for
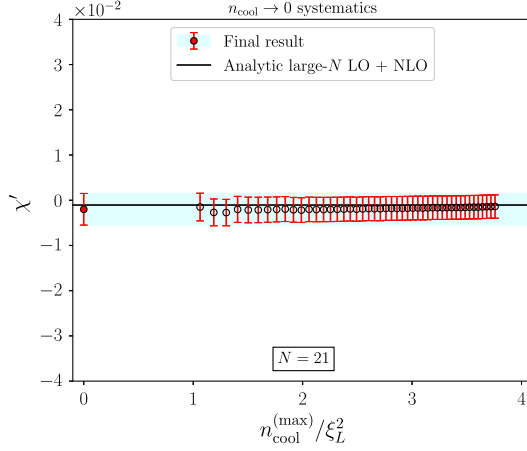
FIG. 8. Results of the zero-cooling extrapolation varying the upper bound of the fit range $n_{\rm cool}^{(\rm max)}/\xi_L^2$ for $N = 21$, obtained by means of a bootstrap analysis. The lower bound was instead kept fixed at $n_{\rm cool}/\xi_L^2 \simeq 0.56$. The shaded area and the full point in $n_{\rm cool}/\xi_L^2 = 0$ represent our final result.
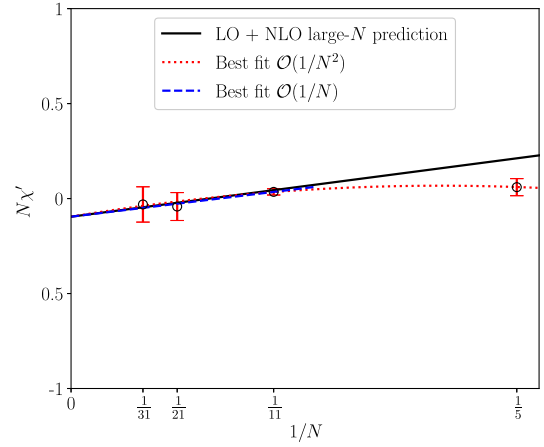

FIG. 9. Large-N behavior of χ' compared to the LO+ NLO analytic $1/N$ prediction. Dotted and dashed lines represent polynomial best fits of our lattice determinations of χ'.

the double extrapolation for different fit ranges, shown in Fig. 8, were estimated by observing the variation of the double limit over such resamplings.

B. The large-N limit of χ'

We repeat the analysis exemplified in the previous section for $N = 5, 11, 31$. Obtained results are reported in Table II, while more details about the double extrapolation for these values of N can be found in the Appendix.

Our aim is now to compare our results with the large-N behavior predicted via the analytic $1/N$ expansion in Eq. (10). Such comparison is shown in Fig. 9. Although our error bars are quite large (with our $N = 21$ and 31 determinations being compatible with 0 within errors), it is clear that our numerical results are in very good agreement with the large-N analytic ones and approach the NLO prediction already for $N \geq 11$.

If we try a best fit of our data for $N\chi'$ with a polynomial in $1/N$, fixing the large-N limit to $e_1' = -3/(10\pi)$,

$$N\chi' = e_1' + e_2'\frac{1}{N} + e_3'\frac{1}{N^2}, \qquad (23)$$

TABLE II. Lattice determinations of χ' as a function of N after the double continuum + zero-cooling extrapolation.

N	χ'
5	0.0120(90)
11	0.0032(15)
21	−0.0020(35)
31	−0.0010(30)

we find $e_2' = 1.44(18)$ (analytic, 1.53671) by fitting up to $\mathcal{O}(1/N)$ terms in the range $N \geq 11$, and $e_3' = -5.9(2.6)$ by fitting up to $\mathcal{O}(1/N^2)$ terms in the range $N \geq 5$ (with e_2' staying within errors). Leaving e_1' as a free parameters gives perfectly compatible results but within larger error bars. These best fits are displayed in Fig. 9 as dashed and dotted lines.

Our result for e_2' is thus in perfect agreement with the large-N analytic computation. We are also able to give a preliminary estimation of e_3', which turns out to be larger by about a factor of 4 and of opposite sign compared to e_2'. These findings match very well with those found for the large-N behavior of the susceptibility χ and of the quartic coefficient b_2 in Ref. [58], where the coefficients of the $1/N$ expansion of these quantities appear to grow in absolute value with alternating signs as the order of $1/N$ is increased. This is not surprising, the $1/N$ expansion being an asymptotic series.

As a final remark, we stress that the difficulty in observing a clear signal above zero for χ' for $N = 21$, 31 is due to the fact that χ' is suppressed in the large-N limit as $1/N$ and is very small already at small N and is thus not related to any intrinsic drawback of any of the methods here employed. Therefore, this fact does not spoil the feasibility of our strategies in more complex models such as $4d$ $SU(N)$ Yang-Mills theories, where such suppression at large N is not expected to occur.

V. CONCLUSIONS

In this paper we have presented a complete lattice investigation of the topological susceptibility slope χ' in $2d$ CP^{N-1} models in the large-N limit. Our main purpose was to test the feasibility of our numerical strategies in view of an application to $4d$ gauge theories, where this

quantity plays an intriguing theoretical and phenomenological role.

Our approach relies on the parallel tempering on boundary conditions to mitigate topological freezing and on a double extrapolation (continuum limit followed by the zero-cooling limit) to correctly reconstruct χ'. This strategy ensures that no relevant UV contribution is lost because of the smoothing method used to properly identify the topological charge of lattice field configurations.

We computed χ' for $N = 5, 11, 21$ and 31 and found that our results are in very good agreement with those obtained from the large-N analytic $1/N$ expansion. Therefore, this confirms the solidity and the feasibility of our numerical methods to compute χ' from the lattice.

For this reason, in the near future we aim at employing such strategies also for $4d$ gauge theories. In particular, our next step will be to compute χ' in the $4d$ SU(3) pure-gauge theory, in view of a lattice investigation of its large-N limit in Yang-Mills theories, which has relevant theoretical interest in relation with the Witten-Veneziano mechanism. In the next future we also plan to perform an investigation of χ' in full QCD, where its value has intriguing phenomenological implications.

ACKNOWLEDGMENTS

APPENDIX: DOUBLE EXTRAPOLATION OF χ' FOR $N = 5, 11, 31$

In Figs. 10–12 we show the double extrapolation of χ' for $N = 5, 11, 31$ as done for $N = 21$ in Sec. IV A. Results are displayed as follows: few examples of continuum extrapolation at fixed value of $n_{\rm cool}/\xi_L^2$, linear extrapolation in $n_{\rm cool}/\xi_L^2$ toward the zero-cooling limit, and systematics related to the zero-cooling best fit.
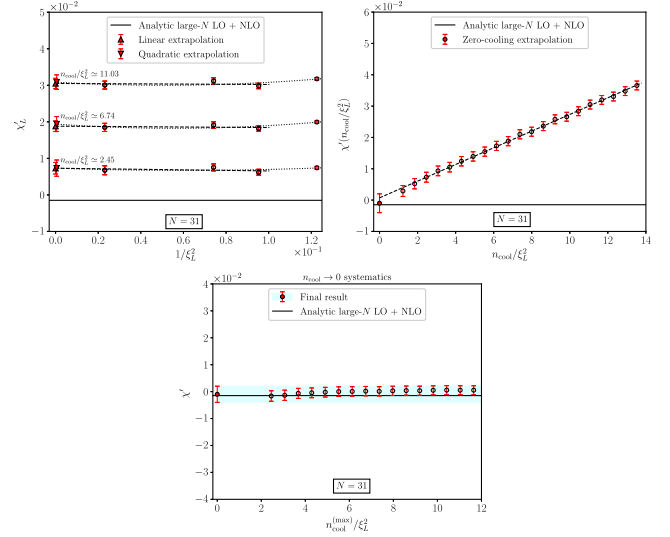

FIG. 10. Figures refer to $N = 31$. Top left: examples of extrapolation toward the continuum limit of χ_L at fixed $n_{\rm cool}/\xi_L^2$. Top right: extrapolation toward the zero-cooling limit with a linear function in $n_{\rm cool}/\xi_L^2$. Bottom: results of the zero-cooling extrapolation varying the upper bound of the fit range $n_{\rm cool}^{\rm (max)}/\xi_L^2$. Final result for χ' is shown as a full point in $n_{\rm cool} = 0$.
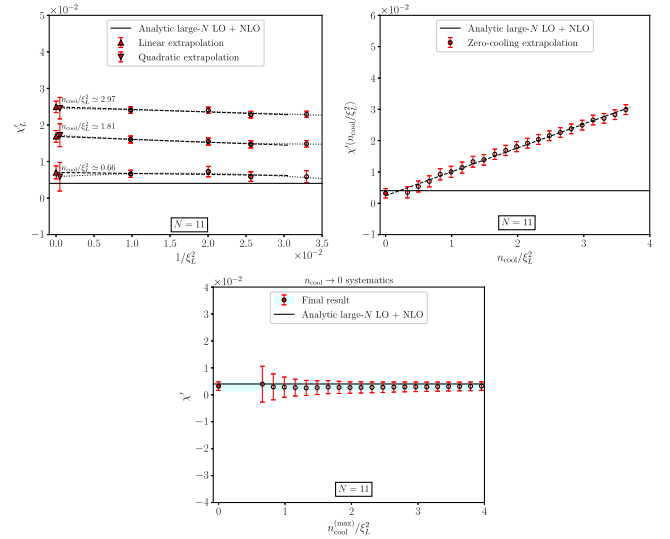
FIG. 11. Figures refer to $N = 11$. Top left: examples of extrapolation toward the continuum limit of χ_L at fixed $n_{\rm cool}/\xi_L^2$. Top right: extrapolation toward the zero-cooling limit with a linear function in $n_{\rm cool}/\xi_L^2$. Bottom: results of the zero-cooling extrapolation varying the upper bound of the fit range $n_{\rm cool}^{\rm (max)}/\xi_L^2$. Final result for χ' is shown as a full point in $n_{\rm cool} = 0$.

FIG. 12. Figures refer to $N = 5$. Top left: examples of extrapolation toward the continuum limit of χ_L at fixed n_{cool}/ξ_L^2. Top right: extrapolation toward the zero-cooling limit with a linear function in n_{cool}/ξ_L^2. Bottom: results of the zero-cooling extrapolation varying the upper bound of the fit range $n_{\text{cool}}^{(\text{max})}/\xi_L^2$. Final result for χ' is shown as a full point in $n_{\text{cool}} = 0$.
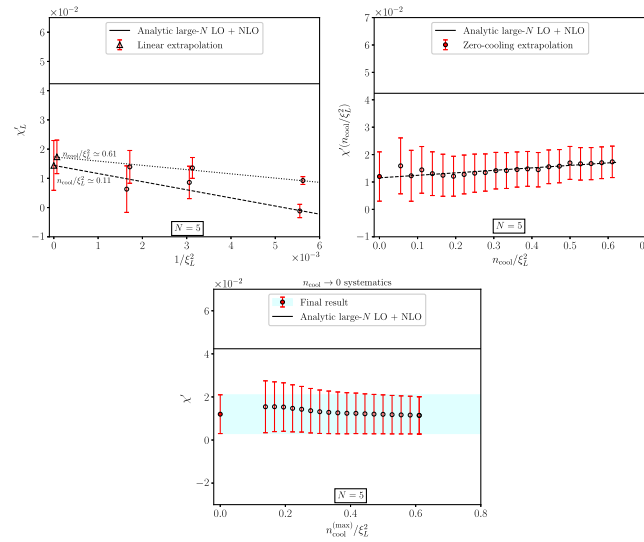
[1] B. Alles, M. D'Elia, A. Di Giacomo, and R. Kirchner, Nucl. Phys. B, Proc. Suppl. **63**, 510 (1998).

[2] E. Vicari, Nucl. Phys. **B554**, 301 (1999).

[3] I. Horvath, A. Alexandru, J. B. Zhang, Y. Chen, S. J. Dong, T. Draper, K. F. Liu, N. Mathur, S. Tamhankar, and H. B. Thacker, Phys. Lett. B **617**, 49 (2005).

[4] E. Vicari and H. Panagopoulos, Phys. Rep. **470**, 93 (2009).

[5] A. Chowdhury, A. K. De, A. Harindranath, J. Maiti, and S. Mondal, J. High Energy Phys. 11 (2012) 029.

[6] H. Fukaya, S. Aoki, G. Cossu, S. Hashimoto, T. Kaneko, and J. Noaki (JLQCD Collaboration). Phys. Rev. D **92**, 111501 (2015).

[7] L. Mazur, L. Altenkort, O. Kaczmarek, and H.-T. Shu, Proc. Sci. LATTICE2019 (**2020**) 219 [arXiv:2001.11967].

[8] L. Altenkort, A. M. Eller, O. Kaczmarek, L. Mazur, G. D. Moore, and H.-T. Shu, Phys. Rev. D **103**, 114513 (2021).

[9] M. B. Mancha and G. D. Moore, arXiv:2210.05507.

[10] E. Witten, Nucl. Phys. **B149**, 285 (1979).

[11] G. Veneziano, Nucl. Phys. **B159**, 213 (1979).

[12] P. Di Vecchia and G. Veneziano, Nucl. Phys. **B171**, 253 (1980).

[13] G. M. Shore and G. Veneziano, Phys. Lett. B **244**, 75 (1990).

[14] G. Shore and G. Veneziano, Nucl. Phys. **B381**, 3 (1992).

[15] B. Alles, A. Di Giacomo, H. Panagopoulos, and E. Vicari, Phys. Lett. B **350**, 70 (1995).

[16] S. Narison, G. M. Shore, and G. Veneziano, Nucl. Phys. **B546**, 235 (1999).

[17] V. Bernard, L. Elouadrhiri, and U.-G. Meissner, J. Phys. G **28**, R1 (2002).

[18] B. Alles, M. D'Elia, and A. Di Giacomo, Nucl. Phys. **B494**, 281 (1997); **B679**, 397(E) (2004).

[19] B. Alles, M. D'Elia, and A. Di Giacomo, Phys. Lett. B **412**, 119 (1997).

[20] L. Del Debbio, L. Giusti, and C. Pica, Phys. Rev. Lett. **94**, 032003 (2005).

[21] L. Del Debbio, H. Panagopoulos, and E. Vicari, J. High Energy Phys. 08 (2002) 044.

[22] M. D'Elia, Nucl. Phys. **B661**, 139 (2003).

[23] L. Del Debbio, G. M. Manca, H. Panagopoulos, A. Skouroupathis, and E. Vicari, J. High Energy Phys. 06 (2006) 005.

[24] B. Lucini, M. Teper, and U. Wenger, Nucl. Phys. **B715**, 461 (2005).

[25] L. Giusti, S. Petrarca, and B. Taglienti, Phys. Rev. D **76**, 094510 (2007).

[26] H. Panagopoulos and E. Vicari, J. High Energy Phys. 11 (2011) 119.

[27] M. Cè, C. Consonni, G. P. Engel, and L. Giusti, Phys. Rev. D **92**, 074502 (2015).

[28] M. Cè, M. Garcia Vera, L. Giusti, and S. Schaefer, Phys. Lett. B **762**, 232 (2016).

[29] C. Bonati, M. D'Elia, and A. Scapellato, Phys. Rev. D **93**, 025028 (2016).

[30] C. Bonati, M. D'Elia, P. Rossi, and E. Vicari, Phys. Rev. D **94**, 085017 (2016).

[31] C. Bonati, M. Cardinali, and M. D'Elia, Phys. Rev. D **98**, 054508 (2018).

[32] F. Burger, E.-M. Ilgenfritz, M. P. Lombardo, and A. Trunin, Phys. Rev. D **98**, 094501 (2018).

[33] C. Bonati, M. Cardinali, M. D'Elia, and F. Mazziotti, Phys. Rev. D **101,** 034508 (2020).

[34] A. Athenodorou and M. Teper, J. High Energy Phys. 11 (2020) 172.

[35] C. Bonanno, C. Bonati, and M. D'Elia, J. High Energy Phys. 03 (2021) 111.

[36] A. Athenodorou and M. Teper, J. High Energy Phys. 12 (2021) 082.

[37] C. Bonanno, M. D'Elia, B. Lucini, and D. Vadacchino, Phys. Lett. B **833,** 137281 (2022).

[38] Bennett, D. K. Hong, J.-W. Lee, C. J. D. Lin, B. Lucini, M. Piai, and D. Vadacchino, Phys. Rev. D **106,** 094503 (2022).

[39] C. Bonati, M. D'Elia, M. Mariti, G. Martinelli, M. Mesiti, F. Negro, F. Sanfilippo, and G. Villadoro, J. High Energy Phys. 03 (2016) 155.

[40] J. Frison, R. Kitano, H. Matsufuru, S. Mori, and N. Yamada, J. High Energy Phys. 09 (2016) 021.

[41] S. Borsanyi *et al.*, Nature (London) **539,** 69 (2016).

[42] P. Petreczky, H.-P. Schadler, and S. Sharma, Phys. Lett. B **762,** 498 (2016).

[43] C. Bonati, M. D'Elia, G. Martinelli, F. Negro, F. Sanfilippo, and A. Todaro, J. High Energy Phys. 11 (2018) 170.

[44] C. Bonanno, G. Clemente, M. D'Elia, and F. Sanfilippo, J. High Energy Phys. 10 (2019) 187.

[45] M. P. Lombardo and A. Trunin, Int. J. Mod. Phys. A **35,** 2030010 (2020).

[46] A. Y. Kotov, A. Trunin, and M. P. Lombardo, Proc. Sci. LATTICE2021 (**2022**) 032 [arXiv:2111.15421].

[47] A. Athenodorou, C. Bonanno, C. Bonati, G. Clemente, F. D'Angelo, M. D'Elia, L. Maio, G. Martinelli, F. Sanfilippo, and A. Todaro, J. High Energy Phys. 10 (2022) 197.

[48] Y.-C. Chen, T.-W. Chiu, and T.-H. Hsieh (TWQCD Collaboration), Phys. Rev. D **106,** 074501 (2022).

[49] M. Campostrini, A. Di Giacomo, and H. Panagopoulos, Phys. Lett. B **212,** 206 (1988).

[50] M. Campostrini, P. Rossi, and E. Vicari, Phys. Rev. D **46,** 2647 (1992).

[51] M. Campostrini, P. Rossi, and E. Vicari, Phys. Rev. D **46,** 4643 (1992).

[52] B. Alles, M. D'Elia, A. Di Giacomo, and R. Kirchner, Phys. Rev. D **58,** 114506 (1998).

[53] L. Del Debbio, G. M. Manca, and E. Vicari, Phys. Lett. B **594,** 315 (2004).

[54] W. Bietenholz, U. Gerber, M. Pepe, and U.-J. Wiese, J. High Energy Phys. 12 (2010) 020.

[55] M. Hasenbusch, Phys. Rev. D **96,** 054504 (2017).

[56] C. Bonati and M. D'Elia, Phys. Rev. E **98,** 013308 (2018).

[57] C. Bonanno, C. Bonati, and M. D'Elia, J. High Energy Phys. 01 (2019) 003.

[58] M. Berni, C. Bonanno, and M. D'Elia, Phys. Rev. D **100,** 114509 (2019).

[59] M. Berni, C. Bonanno, and M. D'Elia, Phys. Rev. D **102,** 114519 (2020).

[60] C. Bonanno, M. D'Elia, and F. Margari, arXiv:2208.00185.

[61] H. Leutwyler, arXiv:hep-ph/0008124.

[62] B. L. Ioffe and A. G. Oganesian, Phys. Rev. D **57,** R6590 (1998).

[63] S. Narison, Sense of beauty in physics: Miniconference in Honor of Adriano di Giacomo on his 70th Birthday (2006), arXiv:hep-ph/0601066.

[64] S. Narison, Nucl. Phys. **A1020,** 122393 (2022).

[65] A. Di Giacomo, Nucl. Phys. B: Proc. Suppl. **23,** 191 (1991).

[66] G. Briganti, A. Di Giacomo, and H. Panagopoulos, Phys. Lett. B **253,** 427 (1991).

[67] A. Di Giacomo, E. Meggiolaro, and H. Panagopoulos, Phys. Lett. B **291,** 147 (1992).

[68] G. Boyd, B. Alles, M. D'Elia, and A. Di Giacomo, in *Proceedings of the 1997 Europhysics Conference on High Energy Physics* (1997), pp. 1028–1033, arXiv:hep-lat/9711025.

[69] A. D'Adda, M. Lüscher, and P. Di Vecchia, Nucl. Phys. **B146,** 63 (1978).

[70] M. Lüscher, Phys. Lett. **78B,** 465 (1978).

[71] M. Shifman, *Advanced Topics in Quantum Field Theory: A Lecture Course* (Cambridge University Press, Cambridge, England, 2012), ISBN 978-1-139-21036-2, 978-0-521-19084-8.

[72] M. Campostrini and P. Rossi, Phys. Lett. B **272,** 305 (1991).

[73] B. Berg, Phys. Lett. **104B,** 475 (1981).

[74] S. Caracciolo and A. Pelissetto, Phys. Rev. D **58,** 105007 (1998).

[75] Y. Iwasaki and T. Yoshie, Phys. Lett. **131B,** 159 (1983).

[76] S. Itoh, Y. Iwasaki, and T. Yoshie, Phys. Lett. **147B,** 141 (1984).

[77] M. Teper, Phys. Lett. **162B,** 357 (1985).

[78] E.-M. Ilgenfritz, M. Laursen, G. Schierholz, M. Müller-Preussker, and H. Schiller, Nucl. Phys. **B268,** 693 (1986).

[79] M. Campostrini, A. Di Giacomo, H. Panagopoulos, and E. Vicari, Nucl. Phys. **B329,** 683 (1990).

[80] B. Alles, L. Cosmai, M. D'Elia, and A. Papa, Phys. Rev. D **62,** 094507 (2000).

[81] M. Albanese *et al.* (APE Collaboration), Phys. Lett. B **192,** 163 (1987).

[82] C. Morningstar and M. J. Peardon, Phys. Rev. D **69,** 054501 (2004).

[83] M. Lüscher, Commun. Math. Phys. **293,** 899 (2010).

[84] M. Lüscher, J. High Energy Phys. 08 (2010) 071; 03 (2014) 092.

[85] C. Bonati and M. D'Elia, Phys. Rev. D **89,** 105005 (2014).

[86] C. Alexandrou, A. Athenodorou, and K. Jansen, Phys. Rev. D **92,** 125014 (2015).

[87] M. Aguado and M. Asorey, Nucl. Phys. **B844,** 243 (2011).